

Guided interactive image segmentation using machine learning and color based data set clustering

Adrian Friebel^{1,*}, Tim Johann², Dirk Drasdo^{2,3}, Stefan Hoehme^{1*}

1 Institute for Computer Science, Leipzig University, Härtelstr. 16–18, 04107, Leipzig, Germany; 2 IfADo - Leibniz Research Centre for Working Environment and Human Factors, Ardeystrasse 67, Dortmund, Germany; 3 Inria Paris & Sorbonne Université LJLL, 2 Rue Simone IFF, 75012, Paris, France; * Corresponding Author

Over the last decades image processing and analysis became one of the key techniques in systems biology and medicine. Today, a multitude of microscopy techniques generates a variety of image types such as two-dimensional whole slide scans, three-dimensional image stacks or time resolved image sequences. Traditional segmentation methods are usually tailor made, targeting a specific physiological entity and image setup in regards to e.g. dimensionality, staining or magnification. Hence, such methods are typically limited in their applicability to differing use cases. Deep learning proved to be an extremely powerful approach, improving performance on all tasks related to image analysis, including segmentation. However, in the life sciences data sets often comprise few images and qualified annotations are not always readily available and expensive to produce, rendering deep learning ineffective. Therefore, it is indispensable to close this gap and develop processing methods that are flexible and therefore can be easily adapted to a variety of image types and diverse tissue structures as well as easy to use, minimizing the need for human intervention.

We present a novel approach that combines machine learning based interactive image segmentation with a two-stage clustering method for identification of similarly colored images enabling efficient batch image segmentation through guided reuse of interactively trained classifiers. The segmentation task is formulated as a supervised machine learning problem working on supervoxels. These visually homogeneous groups of voxels are characterized using local color, edge and texture features. Classifiers are interactively trained from sparse annotations in a iterative process of annotation refinement. Resulting models can be used for batch processing of previously unseen images. However, due to systemic discrepancies of image colorization classifier reusability is typically limited. By clustering a set of images into subsets of similar colorization, considering characteristic dominant color vectors obtained from the individual images it is possible to identify a minimal set of prototype images eligible for interactive segmentation. We demonstrate that limiting the reuse of pre-trained classifiers to images in the same color-cluster significantly improves the average segmentation performance of batch processing.

The described methods are implemented in our free image processing and quantification software TiQuant released alongside this publication.

Introduction

Advances in imaging technology led to a diversification of microscopy techniques enabling examination of a broad spectrum of biological questions and thus established imaging and image analysis as one of the main pillars of bioscience. Optical microscopy in combination with (immuno)histochemical and immunofluorescent staining allows for visualization of tissue and specific physiological entities. Therefore, these techniques are widely used in a clinical setting for medical diagnosis, e.g. using histological sections of biopsies, as a means to study physiological and pathological tissue architecture states, e.g. using 3D volumetric confocal microscopy (Hammad et al. 2014; Friebel et al. 2015; Hoehme et al. 2010), as well as tissue-scale or intracellular processes, e.g. by time resolved two-photon microscopy (Vartak et al. 2019). Computer based image analysis is in many use cases necessarily preceded by detection or pixel-accurate segmentation of objects of interest. The most basic segmentation technique, manual pixel-accurate labeling, is time consuming, inconsistent and in many use cases, such as segmentation of e.g. blood vessels in volumetric datasets, not practically feasible. A multitude of (semi-)automatic image processing methods have been proposed, including e.g. intensity-thresholding and morphological operators (Hammad et al. 2014; Hoehme et al. 2010), region-based methods (Lopez et al. 1999) or deformable models (McInerney and Terzopoulos 1996). These methods are usually tailored towards a specific image setup (i.a. image dimensionality, magnification, staining) and/or object class (e.g. nuclei, blood vessels, necrotic tissue) and as such are typically limited in their applicability to differing use cases. Additionally, method parametrization to cope with image variability is often challenging and time consuming. More recently, shallow and deep machine learning methods were successfully applied to pixel-accurate image segmentation (Lucchi et al. 2012; Ren and Malik 2003; Ronneberger, Fischer, and Brox 2015; Ciresan et al. 2012). By learning object appearance from training examples these methods allow for incorporation of subtle expert knowledge, are less restricted regarding image or object class specifics and minimize parameterization complexity.

We aim to provide a tool set for (i) interactive segmentation of single images with minimal user intervention, where a discriminative model is learned from sparse annotations, as well as (ii) effective batch image segmentation of similar, unseen images through reuse of trained models.

Deep learning proved to be an extremely powerful approach improving performance on all tasks related to image analysis (Krizhevsky, Sutskever, and Hinton 2012; He et al. 2017; Ronneberger, Fischer, and Brox 2015; Long, Shelhamer, and Darrell 2015). This is mostly due to its ability of operating directly on the input image and implicitly learning features of increasing complexity. The price for finding a suitable feature space in addition to the decision surface itself is a high demand for training data and long training times. Therefore, while deep learning approaches are able to achieve superior performance their applicability in use cases with very low image counts or for interactive image segmentation is limited. In contrast, traditional, so called shallow, machine learning approaches such as random forests or support-vector machines, rely on handcrafted features. While this limits versatility, as engineered features need to represent the learning problem at hand, finding only a decision surface in a given feature space greatly simplifies the learning task. Thereby, relatively few training examples and short training times are required, which makes these shallow methods eminently suitable for interactive segmentation.

A number of interactive segmentation approaches and software packages that facilitate machine learning have been published in recent years. A supervoxel-based approach for segmentation of mitochondria in volumetric EM images was developed by (Lucchi et al. 2012), though the published executable software and code encompassed only the supervoxel algorithm *SLIC*. SuRVos (Luengo et al. 2017) is a software for interactive segmentation of 3D images using a supervoxel-based hierarchy, which lays a focus on segmentation of noisy, low-contrast EM datasets. The extendable software package Microscopy Image Browser (Belevich et al. 2016) allows for processing of multidimensional datasets and features a selection of conventional processing algorithms, several region selection methods aiding manual segmentation, and methods for semi-automatic segmentation, including a supervoxel-based classification approach. FastER (Hilsenbeck et al. 2017) is designed specifically for cell segmentation in grayscale images, using features that are very fast to compute. The Fiji plugin Trainable Weka Segmentation (Arganda-Carreras et al. 2017) is a tool for pixel classification in 2D and 3D images using a broad range of features. Ilastik (Berg et al. 2019) provides a streamlined user interface with workflows for i.a. image segmentation, object classification and tracking as well as a sophisticated on-demand back end enabling processing of images with up to five dimensions that are larger than available RAM. Its segmentation workflow employs a random forest classifier for pixel classification from local features such as color, edge-ness and texture at different scales.

Most of these interactive segmentation tools allow for reuse of trained classifiers on new, unseen images. However, due to the variability of image appearance, even for sets of images that were acquired following a standard protocol, classifier reuse is usually a trial-and-error procedure and quickly becomes cumbersome for larger image sets. One of the main contributing factors to image quality variability are systemic discrepancies of colorization that can be attributed to minor deviations in the image acquisition process (e.g. sample preparation procedure, imaging settings, condition of the imaged subject). Since color information is used in various ways as a feature by all mentioned segmentation tools that target colored images, degraded prediction accuracy is to be expected for images with variational colorization.

In this paper, we propose a combined approach for (i) interactively supervised image segmentation from sparse annotations and (ii) guided reuse of thereby trained classifiers on unseen images for efficient batch processing. These general methods for segmentation of two- and three-dimensional images are integrated into our image processing software TiQuant which encompasses various processing tools specific for liver tissue segmentation from 3D confocal micrographs as well as the corresponding analysis functionality (Hammad et al. 2014; Friebel et al. 2015). (i) We formulate interactive pixel-accurate segmentation as a machine learning problem working on superpixels using random forests or support vector machines as classifiers. Dimensionality reduction through use of superpixels, precomputation of superpixel features and a convenient graphical user interface enable rapid, intuitive refinement of training annotations by iterative correction of classification errors or uncertainties. (ii) We introduce a color-based image clustering method that enables automated partitioning of image sets into subsets of similarly colored images. A corresponding number of so called prototype images is identified which serve as eligible candidates for interactive training of classifiers for within-subset reuse.

We evaluate the interactive image segmentation method as well as the color-based image clustering strategy to guide classifier reuse using a previously published dataset consisting of 22 brightfield micrographs of mouse liver tissue with corresponding manual nuclei annotations (Hoehme et al. 2010). We show that the interactive approach outperforms a human annotator and a comparable state-of-the-art software and that limiting classifier reuse to similarly colored images greatly enhances performance compared to reuse on images of differing colorization, yielding results close to the level of a human annotator.

Method

The general workflow of segmenting an image with our superpixel-based approach is split from a user perspective into a preprocessing step and the interactive training, prediction and segmentation steps, that need direct user intervention and might need to be revisited iteratively for refinement in order to approach a segmentation of sufficient quality (see *Fig 1*).

In the preprocessing step the image is partitioned into superpixels and descriptive features are computed for them. A single parameter, the superpixel size, needs to be adjusted by the user to ensure superpixels fit the objects of interest. This step is computationally expensive compared to the interactive steps, but is usually only performed once per dataset.

In the next step the user annotates exemplary fore- and background regions directly in the original image to generate a training database. Subsequently, a classifier is fitted to the training data and class membership probability estimates are predicted for all superpixels of the dataset. In the final step a segmentation is generated based on the probability estimates and post-processing might be applied for refinement.

If segmentation quality is insufficient, the user can go back to the training step, to provide more training data, especially for regions that were poorly segmented. Thereby, high-quality segmentations can be quickly generated by iterative annotation refinement.

Trained classifiers can be used for prediction on unseen images, eliminating the need for producing training data for every image. However, since color descriptors are among the learned features, prediction quality on unseen images strongly depends on color similarity with the training image. By clustering a dataset of images into subsets based on their dominant colors, the process of identifying training images and qualified candidate images for classifier reuse is aided.

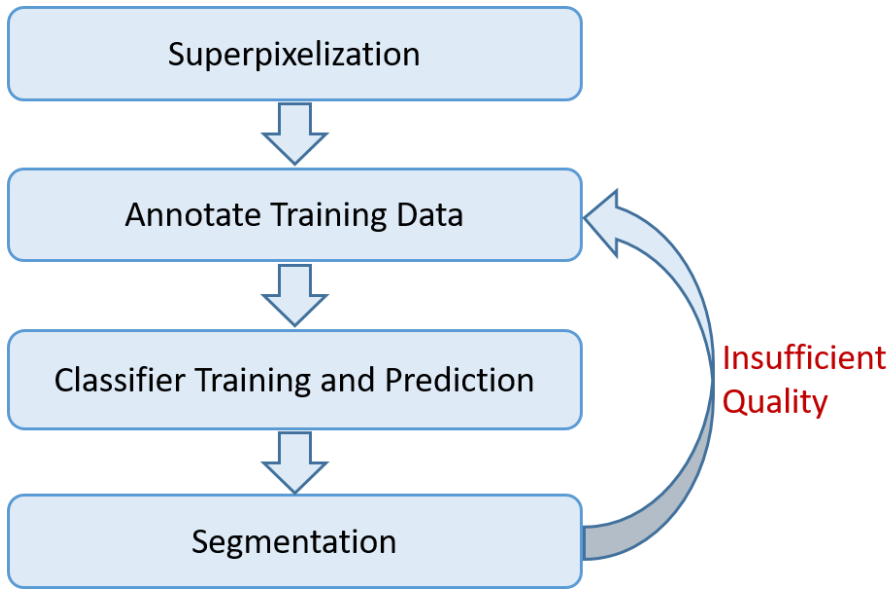


Figure 1: Workflow of our superpixel-based image segmentation approach from a user perspective.

Superpixel initialization

Initially, an oversegmentation into perceptually homogeneous regions, so called supervoxels, is generated.

The term supervoxel (respectively superpixel in 2D) was introduced in (Ren and Malik 2003), who proposed to use oversegmentation, i.e. the process of segmenting an image so that the objects of interest themselves are split into distinct regions, as a preprocessing step to reduce image complexity while preserving most of the structure necessary for segmentation at the scale of interest. Individual supervoxels group voxels into visually meaningful building blocks, which are, depending on the chosen generative approach and parametrization, of more or less similar size and compactness. They reduce dimensionality of data without sacrificing much information, thereby greatly reducing computational cost of subsequent image processing steps and allow for computation of local features such as color histograms and texture. To date a multitude of different supervoxel algorithms exist, which can be categorized by their high-level approach, into e.g. graph-based, density-based and clustering-based algorithms (Stutz, Hermans, and Leibe 2018).

We use the *SLIC0* (“*Superpixels – IVRL*” n.d.) variant of the clustering-based algorithm *simple linear iterative clustering (SLIC)* (Achanta et al. 2012), due to its comparatively strong performance regarding Boundary Recall and Undersegmentation Error (Stutz, Hermans, and Leibe 2018) and its memory and runtime efficiency (Achanta et al. 2012). Its iterative nature

enables straightforward runtime restriction and provides direct control over the number of generated superpixels. *SLIC* is an adaptation of k-means clustering (Lloyd 1982) with two main distinctions: i) The search space is reduced to a region proportional to the superpixel size, yielding a complexity linear in the number of pixels and independent of superpixel number. ii) The used weighted distance measure combines color and spatial proximity, providing control over size and compactness of resulting superpixels. Its variant *SLIC0* adaptively chooses the superpixel compactness, thereby reducing free parameters to number of superpixels, or superpixel size, respectively. Examples for superpixel oversegmentations can be seen in *Fig 2*. The algorithm was implemented as an ITK filter and extended to work in three dimensions. A superpixel oversegmentation is represented as a list of lists of pixels in run-length encoding, which constitute the individual superpixels, as well as a graph, in which vertices represent superpixels and edges signify neighboring pairs of superpixels. This dual representation allows for access to individual superpixels, their constituent pixels, features and spatial relationships. The superpixel features comprise local and neighborhood color histograms, edge-ness over several spatial scales, as well as texture descriptors (detailed description in *SI Appendix*), yielding a feature vector with a total of 138 entries. Feature categories can be disabled by the user to speed up processing.

Interactive training data generation

For training data generation TiQuant provides a graphical user interface that allows visualization of and interaction with image data. The user can draw directly on top of the image in order to denote exemplary regions for the classes to be segmented. Superpixels in the annotated regions are collected and their feature vector together with the annotated class are written into a training database. For examples of how training data annotation looks in the software, see *Fig 2*.

Supervoxel-Classification

We use Support Vector Machines (SVM) and Random Forests (RF) classifiers for learning superpixel's class membership.

The user provided training data summarized in the training database is split in a 70:30 ratio into a training and a test set. The split is done in a stratified fashion to ensure the preservation of relative class frequencies. Feature vectors are normalized, by subtracting mean and scaling to unit variance independently on each feature component, in order to ensure comparable feature scales.

Optionally, hyper-parameter optimization is performed on the chosen classifier to tune classifier parameters, that are not directly learnt, to the observed data patterns. In order to limit execution time while retaining explorative quality of an exhaustive Grid Search the optimization is done using Random Search which tests a fixed number of parameter settings sampled from given distributions (Bergstra and Bengio 2012). The search is performed on the training split with 5-fold stratified cross-validation.

SVMs are setup to provide calibrated probabilistic class membership estimates by using Platt Scaling (Platt and Others 1999), which fits an additional sigmoid function to map SVM scores to probabilities by a 5-fold cross-validation on the training split. Thereby calibrated SVM output can be interpreted as confidence levels. RFs provide probabilistic estimates per default. Those can be optionally calibrated, using Platt Scaling or the non-parametric Isotonic Regression approach (Barlow 1972). Empirical results show that SVMs and RFs are among the models that predict the best probabilities after calibration (Niculescu-Mizil and Caruana 2005). The Brier score was used for classifier evaluation during calibration, since it is a proper scoring rule that measures the accuracy of probabilistic predictions and as such is a measure for calibration (Gneiting and Raftery 2007).

In many cases user provided training data will be imbalanced, with relatively more samples of the background compared to the foreground class. To account for this mismatch, besides using the stratified version of cross-validation, training samples are weighted during training phase, where the weight is inversely proportional to class frequency, and appropriate scoring functions are used for classifier evaluation. The Random Search algorithm used for hyper-parameter optimization uses the balanced accuracy score (Brodersen et al. 2010) to evaluate the performance of the optimized classifier on the test splits during cross-validation.

The optionally optimized and calibrated classifier is trained on the training split and evaluated on the unseen test split to assess its performance. Subsequently, the classifier is trained on the whole data corpus provided by the user and the resulting trained classifier is used to predict the class membership probability estimates of all superpixels of the dataset. Exemplary probability maps are shown in Figure 2.

Segmentation

A naive thresholding is applied to map the probabilistic estimates to binary class-membership, which by default is set to the value of 50%, but can be tuned by the user. The resulting segmentation can be post-processed using three optional filters. The first post-processing step

allows for removal of isolated foreground objects smaller than a specified foreground object size. Vice-versa it allows for filling of holes in the foreground objects that are smaller than a specified background object size. This simultaneous object removal and hole filling is done iteratively until no superpixels change class membership. Additionally, a morphological closing operator followed by an opening operator can be applied, to smooth corners and jagged surfaces. Both operators are topology preserving and thus do not separate a connected foreground object or merge disconnected foreground objects (Beare and Jackway 2011). Finally, the watershed algorithm may be applied in order to split artificially connected objects such as e.g. nuclei (Malpica et al. 1997).

Figure 2 shows two exemplary segmentations.

Color-based image clustering

The aim of the proposed image clustering method is to automatically partition a set of biomedical images acquired under comparable conditions into image subsets that exhibit similar colorization. Thereby, guiding the selection of training images and matching images for classifier reuse, to minimize manual annotation effort. The underlying assumption is that minor procedural discrepancies in the image acquisition process introduce systemic changes of coloring. Possible causes comprise slight variations between sample preparation sessions (e.g. affecting staining penetration depth, thus color saturation), minor deviations in imaging settings between imaging sessions (e.g. affecting brightness and contrast), as well as differing conditions of the imaged subjects (e.g. healthy vs. impaired tissue).

In a first step images are analysed for their dominant colors. This process, also known as palette design, is one of two phases of color quantization, an operation used for e.g. image compression. It has been shown, that k-means clustering (Lloyd 1982) is an effective method for this task (Kasuga, Yamamoto, and Okamoto 2000; Celebi 2009). In order to identify a vector of the k_c most dominant colors of an image, each pixel's RGB color vector is interpreted as a data point in 3D space. Instead of starting with fully random cluster centers the K-Means++ initialisation scheme (Arthur and Vassilvitskii 2006) is used, as it has been demonstrated to improve effectiveness for this task (Celebi 2009). According to Lloyd's algorithm (Lloyd 1982), each color data point is assigned to the closest cluster center and for each of the k_c resulting color clusters the cluster centers are updated as the mean of all data points assigned to them. These two steps are repeated until convergence or until a maximal number of iterations is

executed, yielding a vector of the k_c most dominant colors that minimize the within-cluster variances (squared Euclidean distances).

Following, the dominant color vectors are sorted. The vectors provided by k-means clustering are ordered by color prevalence, i.e. the number of pixels that are assigned to a respective color cluster. This ordering however is susceptible to changes in image composition, so that e.g. the size or number of physiological entities influences the rank of the color cluster(s) they are assigned to. In order to make dominant color vectors of different images more comparable we sort them. Sorting is done component-wise on the RGB vectors.

Finally, the images of a dataset are partitioned into subsets with similar dominant color vectors. Our approach extends previous work, in which color moments (Maheshwary and Srivastav 2008) or histograms (Malakar and Mukherjee 2013) were used as image descriptors for k-means based image clustering. Each image is represented by its $3*k_c$ dimensional sorted dominant color vector. K-means clustering is applied to this set of data points yielding k_i clusters, minimizing the within-cluster variances of the sorted dominant color vectors. The images with the smallest Euclidean distance to their respective cluster center are recommended as training images for their image cluster.

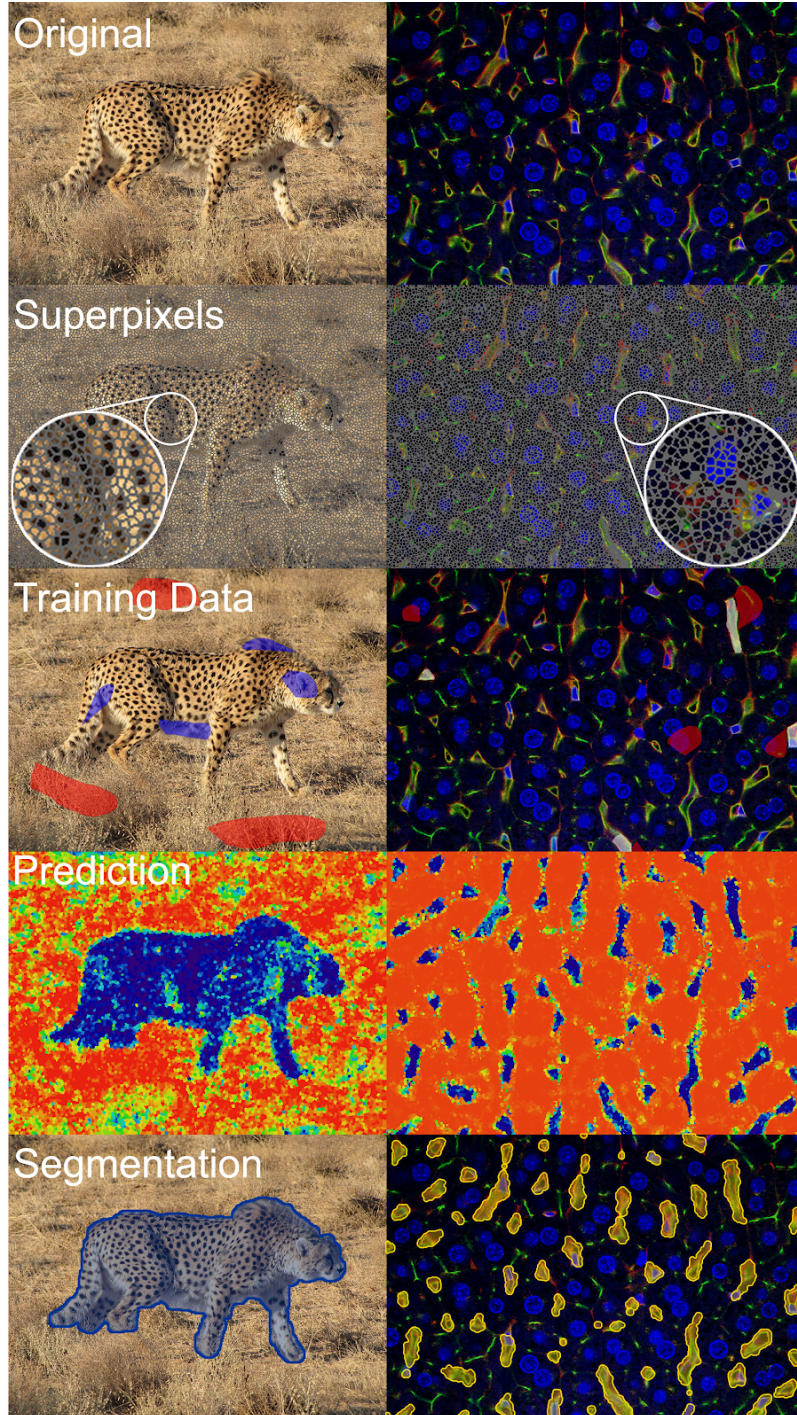


Figure 2: Illustration of superpixel-based image segmentation procedure on a two-dimensional image of a cheetah (left) and a three-dimensional confocal micrograph of liver tissue in which blood vessels were segmented (right). Training data for the background class is colored red in both instances, while the foreground class is colored blue in the left and white in the right example. Class membership probabilities in the prediction row are illustrated using a color mapping ranging from red (low chance of being foreground) over yellow to blue (high chance of being foreground). The segmentation is visualized by a blue overlay on the left, and a yellow overlay on the right.

Experiments

Validation

We validated the superpixel-based segmentation method exemplarily on a dataset consisting of 22 paraffin slices of mouse livers imaged using brightfield microscopy that were manually annotated and subsequently analysed to study the process of tissue regeneration after intoxication with CCl₄ (Hoehme et al. 2010). The slices were immunostained for BrdU positive nuclei to visualize proliferation and the images are centered on a central vein, encompassing one liver lobule, which is the basic building block of liver tissue. They were taken from a control and at 7 different time points after administration of CCl₄, which causes a necrotic lesion in the area around the central vein. Over the covered time period this lesion is gradually closed by invading proliferating liver cells. The images were originally annotated by hand by a single trained person, marking the outlines of the lobule as well as all individual nuclei within it. The analysis based on these manual segmentations was used in (Hoehme et al. 2010) for parametrization of a spatio-temporal model of a liver lobule. We reuse this dataset for method validation as it is representative for many image segmentation tasks in a biomedical context, which are characterized by small total number of available images, varying appearance of images (e.g. variations between sample preparation / imagining sessions, different conditions of imaged subject such as physiological, impaired and regenerating tissue), varying appearance of segmentation targets (e.g. non/proliferating nuclei, cell type dependent nuclei shape) and local image imperfections (e.g. entrapped air, blurring, staining variations).

Close examination of the original annotations revealed several inaccuracies and inconsistencies (Fig. 3A), therefore we reassessed all 22 images thoroughly to generate a final gold standard. This gold standard, as the original annotation, is not a pixel-wise labeling, but rather represents each nucleus, that lies within the confines of the annotated lobule boundaries, as a 2D pixel coordinate. As a measure for the accuracy of a segmentation we use the F₁ score, thereby considering both precision and recall. The underlying numbers of true positives (tp), false positives (fp) and false negatives (fn) are quantified based on a object-wise mapping of gold standard to segmentation (detailed explanation in *SI Appendix*). The measured scores are used for validation and comparison of segmentations from manual annotation (Fig. 3A), semi-automated superpixel-based processing (Fig. 3B), intra- and inter-cluster reuse of

pre-trained classifiers as well as the state-of-the-art tool ilastik (Berg et al. 2019) as a reference point.

For validation of the superpixel-based approach each image was partitioned into approximately 50k superpixels of size 8x8 pixels and each superpixel was analyzed for all available features, encompassing gradient magnitude, Laplacian of Gaussian, local and neighborhood color histograms as well as texture features.

In order to evaluate the suitability of our tool for interactive segmentation, appropriate training data was produced for each of the 22 images manually by annotation (following workflow Fig. 1). Per image a random forest classifier was tuned using hyperparameter optimization with 5-fold stratified cross-validation, then trained and probability calibrated, if beneficial. The final classifiers were applied to the respective image, predicting superpixel's class memberships. The corresponding segmentations were post-processed, by removing objects smaller than three superpixels, smoothing of boundaries of segmented nuclei and finally by applying the watershed algorithm to split up clusters of nuclei into individual objects.

Subsequently, to evaluate how well the trained classifiers generalize to unseen images and whether a restriction to images of similar coloring improves performance we cluster the image set into $k_i=6$ subsets. Image clustering uses sorted dominant color vectors with $k_c=5$ colors. The images with the smallest euclidean distance to their cluster center were selected as cluster prototype images. The previously trained classifiers of these prototype images were applied (i) *intra-cluster* to all other images in the respective cluster and (ii) *inter-cluster* to all images not belonging to the respective cluster. Segmentation post-processing was done as described before.

We compare our approach with established image processing software ilastik. In order to achieve comparable results we used the 'Pixel Classification + Object Classification' workflow. All 37 predefined features were selected for training. The training annotations created with our software were imported and a object size filter was used for segmentation post-processing.

The results of the method validation can be seen in Table 1. The best result was achieved by our method, when providing dedicated training data for each image. The initial manual segmentation and intra-cluster reuse of pre-trained classifiers achieved comparable scores, indicating that the restriction of classifier reuse on similarly colored images is able to produce human-grade results, although, as the higher variance indicates, segmentation quality is less reliable. Reusing classifiers on images with differing coloring generally decreases segmentation

quality greatly, as it was expected given the importance of color information. Ilastik performed slightly better than the pre-trained classifiers on intra-cluster images.

Method	$\text{median}(F_1)$	$\sigma(F_1)$
manual	0.9021	0.027
semi-automatic	0.9297	0.013
intra-cluster	0.9018	0.044
inter-cluster	0.6484	0.245
Ilastik (Berg et al. 2019)	0.9079	0.022

Table 1: Comparison of different segmentation methods on 22 images. Bold indicates the best performance.

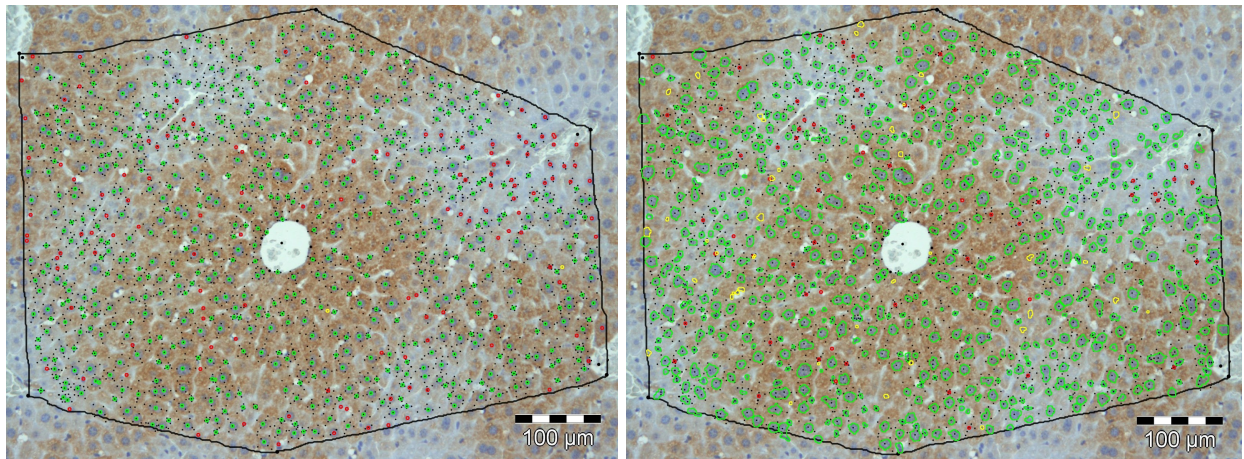


Figure 3: (A) Exemplary visual comparison of manual segmentation with gold standard (GS): Correctly segmented nuclei (true positives) (bright green); Incorrectly segmented nuclei (false positives) (yellow); Items not segmented as nuclei (false negatives) (red). Outlines generated from dilated 2D pixel coordinates. **(B)** Exemplary visual comparison of semi-automatic segmentation with GS: Coloring as in (A). Outlines generated from object masks.

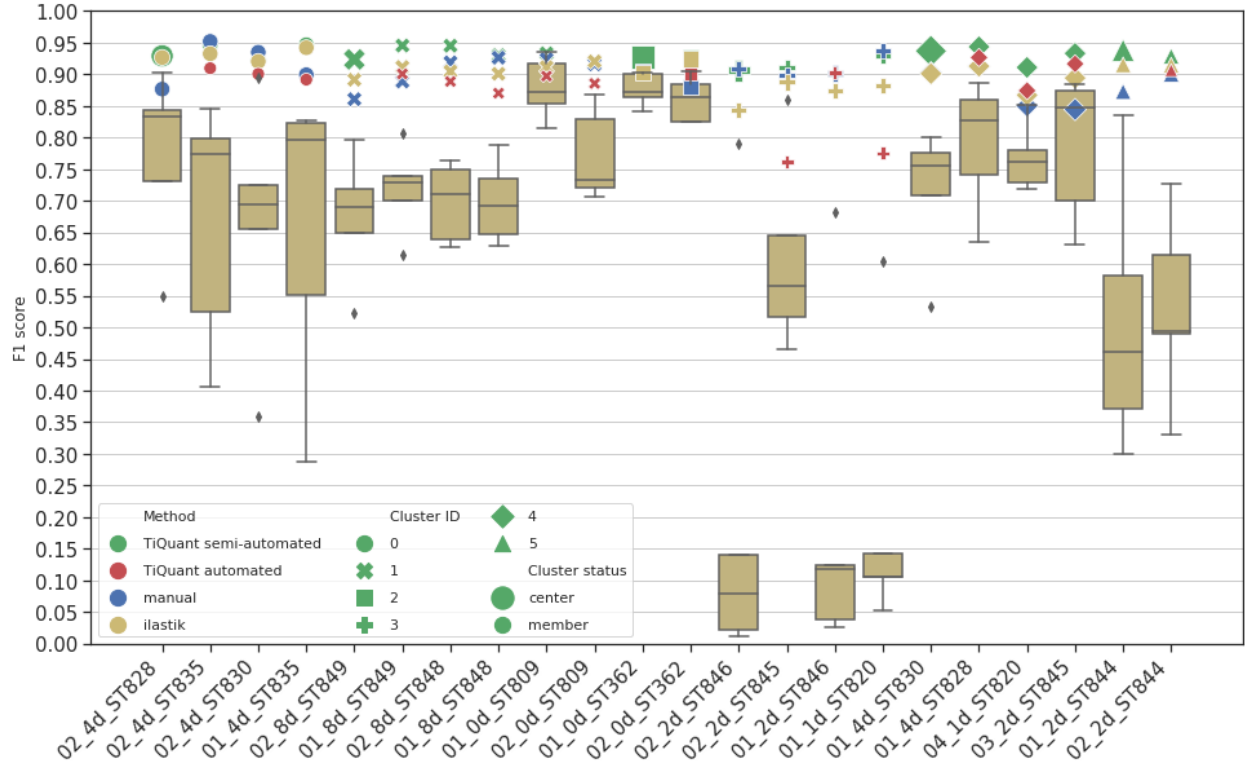


Figure 4: Per image comparison of different segmentation methods: Manual annotation (blue), semi-automated superpixel-based processing (green), intra-cluster reuse of pre-trained classifier (red), inter-cluster reuse of pre-trained classifiers (box) and ilastik's 'Pixel Classification + Object Classification' workflow (Berg et al. 2019) (yellow). For intra-cluster performance analysis the classifier trained on the cluster prototype image (leftmost) was reused on the remaining images of the respective cluster. Therefore, the cluster prototype image has no intra-cluster score. Inter-cluster performances are given as boxplot summarizing the performance of classifiers of all other clusters.

Runtime evaluation

A detailed discussion of aspects of computational performance is given in the *SI Appendix*.

The interactive processing steps training and prediction are independent of pixel count and linear in the number of superpixels. The segmentation step is linear in pixel count and number of superpixels. Exemplarily, execution times for an image with 100M pixels and 100k superpixels are ~2min and 9min for superpixel generation without and with feature generation. Training database generation, prediction and segmentation were completed in 5sec, 12sec and 51sec, respectively. The analysis was done on a Intel Core i9-7900X with 10 logical cores at a 3.3 GHz clockspeed with 64 GB RAM.

Discussion

Interactive image segmentation fills a niche in the spectrum of image processing approaches addressing applications where data sets are small, containing few images, and/or training annotations are not readily available and detailed analysis of objects of interest is the aim. These conditions are true for many use cases in e.g. biological and medical image processing where oftentimes pixel-accurate segmentations of physiological entities from two or three dimensional images are required in order to allow for e.g. volume, contact area or network measurements. Under these circumstances custom made image processing solutions that target a specific physiological entity in a specific image setup are still a widespread approach. However these tailor made solutions cause considerable development overhead compared to interactive solutions based on 'shallow' machine learning that can be adapted to new data through training. Adaptation through learning from image annotations also greatly simplifies the application of such solutions, eliminating the need for technical parameters and thus flattening the learning curve for users. But even if a large data set is available, theoretically enabling deep learning, interactive image segmentation is instrumental in producing training data by greatly reducing the necessary user interactions and thus cost of manual annotation.

The chosen superpixel approach using the *SLIC0* algorithm is especially suited as a basis for responsive, interactive segmentation due to its single free parameter, making it easy to use, and its dimensionality reduction characteristic, minimizing processing times and memory consumption. The latter effect is especially pronounced if the objects of interest are highly resolved, and is increasingly diminished, if their size or thickness approaches pixel resolution. Furthermore, for objects with fluent boundaries or low resolution images the alignment of superpixels to object boundaries can be suboptimal and pixel-level classification might provide higher segmentation accuracy in boundary areas.

While learning discriminative models using a handcrafted feature space decreases the number of necessary training samples allowing for learning from sparse annotations, and thus rapid interactive segmentation, it also limits versatility. The features we implemented are designed for application to color images and might be insufficient in representing a learning problem formulated on grayscale images (e.g. EM or CT images), for which suitable features would have to be developed.

In order to further decrease human intervention interactively trained classifiers can be reused on unseen images. The downside of learning from sparse annotations on single images is a

hampered generalization ability, especially when trained models are used to segment images of differing colorization. We demonstrated that limiting classifier reuse to similarly colored images improved average performance for the validation data set significantly, thereby improving suitability of interactive image segmentation for processing of moderately sized data sets.

Conclusion

We have presented a novel approach that combines machine learning based interactive image segmentation using supervoxels with a clustering method for identification of similarly colored images enabling guided reuse of interactively trained classifiers.

Biological image datasets usually exhibit significant inter-image color variability due to minor discrepancies in the acquisition process. While most interactive image segmentation tools allow for reuse of trained classifiers, degraded segmentation accuracy is to be expected for images with deviating color palettes, given their reliance on very sparse training data and color-based features. Efficient processing of larger quantities of images is thereby greatly hampered.

With our approach a dataset is clustered into subsets of image with similar colorization allowing for identification of a corresponding set of representative images, suited for interactive segmentation and thus generation of subset specific classifiers.

We have demonstrated that our interactive image segmentation approach is able to achieve results of comparable accuracy compared to a human annotator and a popular interactive segmentation tool. Furthermore, we have shown, that limiting reuse of interactively trained classifiers to unseen images of the same subset, thus images with similar colorization, significantly improved accuracy compared to non-discriminative reuse.

The proposed strategy helps to make interactive segmentation from sparse annotations a viable option even for datasets with large numbers of images by guiding the segmentation process minimizing cost-intensive manual labor.

The described methods are implemented in our free image processing and analysis software TiQuant.

Bibliography

- Achanta, Radhakrishna, Appu Shaji, Kevin Smith, Aurelien Lucchi, Pascal Fua, and Sabine Süstrunk. 2012. "SLIC Superpixels Compared to State-of-the-Art Superpixel Methods." *IEEE Transactions on Pattern Analysis and Machine Intelligence* 34 (11): 2274–82.
- Arganda-Carreras, Ignacio, Verena Kaynig, Curtis Rueden, Kevin W. Eliceiri, Johannes Schindelin, Albert Cardona, and H. Sebastian Seung. 2017. "Trainable Weka Segmentation: A Machine Learning Tool for Microscopy Pixel Classification." *Bioinformatics*. <https://doi.org/10.1093/bioinformatics/btx180>.
- Arthur, David, and Sergei Vassilvitskii. 2006. "K-Means++: The Advantages of Careful Seeding." Stanford. <http://ilpubs.stanford.edu:8090/778>.
- Barlow, Richard E. 1972. "Statistical Inference under Order Restrictions; the Theory and Application of Isotonic Regression." <http://www.sidalc.net/cgi-bin/wxis.exe/?IsisScript=COLPOS.xis&method=post&formato=2&cantidad=1&expresion=mfn=002313>.
- Beare, R., and P. Jackway. 2011. "Parallel Algorithms via Scaled Paraboloid Structuring Functions for Spatially-Variant and Label-Set Dilations and Erosions." In *2011 International Conference on Digital Image Computing: Techniques and Applications*, 180–85.
- Belevich, Ilya, Merja Joensuu, Darshan Kumar, Helena Vihinen, and Eija Jokitalo. 2016. "Microscopy Image Browser: A Platform for Segmentation and Analysis of Multidimensional Datasets." *PLoS Biology* 14 (1): e1002340.
- Bergstra, James, and Yoshua Bengio. 2012. "Random Search for Hyper-Parameter Optimization." *Journal of Machine Learning Research: JMLR* 13 (10): 281–305.
- Berg, Stuart, Dominik Kutra, Thorben Kroeger, Christoph N. Straehle, Bernhard X. Kausler, Carsten Haubold, Martin Schiegg, et al. 2019. "Ilastik: Interactive Machine Learning for (bio)image Analysis." *Nature Methods*. <https://doi.org/10.1038/s41592-019-0582-9>.
- Brodersen, K. H., C. S. Ong, K. E. Stephan, and J. M. Buhmann. 2010. "The Balanced Accuracy and Its Posterior Distribution." In *2010 20th International Conference on Pattern Recognition*, 3121–24.
- Celebi, M. E. 2009. "Effective Initialization of K-Means for Color Quantization." In *2009 16th IEEE International Conference on Image Processing (ICIP)*, 1649–52.
- Ciresan, Dan, Alessandro Giusti, Luca M. Gambardella, and Jürgen Schmidhuber. 2012. "Deep Neural Networks Segment Neuronal Membranes in Electron Microscopy Images." In *Advances in Neural Information Processing Systems 25*, edited by F. Pereira, C. J. C. Burges, L. Bottou, and K. Q. Weinberger, 2843–51. Curran Associates, Inc.
- Friebel, Adrian, Johannes Neitsch, Tim Johann, Seddik Hammad, Jan G. Hengstler, Dirk Drasdo, and Stefan Hoehme. 2015. "TiQuant: Software for Tissue Analysis, Quantification and Surface Reconstruction." *Bioinformatics* 31 (19): 3234–36.
- Gneiting, Tilman, and Adrian E. Raftery. 2007. "Strictly Proper Scoring Rules, Prediction, and Estimation." *Journal of the American Statistical Association* 102 (477): 359–78.
- Hammad, Seddik, Stefan Hoehme, Adrian Friebel, Iris von Recklinghausen, Amnah Othman, Brigitte Begher-Tibbe, Raymond Reif, et al. 2014. "Protocols for Staining of Bile Canicular and Sinusoidal Networks of Human, Mouse and Pig Livers, Three-Dimensional Reconstruction and Quantification of Tissue Microarchitecture by Image Processing and Analysis." *Archives of Toxicology* 88 (5): 1161–83.
- He, Kaiming, Georgia Gkioxari, Piotr Dollar, and Ross Girshick. 2017. "Mask R-CNN." 2017

- IEEE International Conference on Computer Vision (ICCV).*
[https://doi.org/10.1109/iccv.2017.322.](https://doi.org/10.1109/iccv.2017.322)
- Hilsenbeck, Oliver, Michael Schwarzfischer, Dirk Loeffler, Sotiris Dimopoulos, Simon Hastreiter, Carsten Marr, Fabian J. Theis, and Timm Schroeder. 2017. "fastER: A User-Friendly Tool for Ultrafast and Robust Cell Segmentation in Large-Scale Microscopy." *Bioinformatics* 33 (13): 2020–28.
- Hoehme, Stefan, Marc Brulport, Alexander Bauer, Essam Bedawy, Wiebke Schormann, Matthias Hermes, Verena Puppe, et al. 2010. "Prediction and Validation of Cell Alignment along Microvessels as Order Principle to Restore Tissue Architecture in Liver Regeneration." *Proceedings of the National Academy of Sciences of the United States of America* 107 (23): 10371–76.
- Kasuga, Hideo, Hiroaki Yamamoto, and Masayuki Okamoto. 2000. "Color Quantization Using the Fast K-Means Algorithm." *Systems and Computers in Japan* 31 (8): 33–40.
- Krizhevsky, Alex, Ilya Sutskever, and Geoffrey E. Hinton. 2012. "ImageNet Classification with Deep Convolutional Neural Networks." In *Advances in Neural Information Processing Systems 25*, edited by F. Pereira, C. J. C. Burges, L. Bottou, and K. Q. Weinberger, 1097–1105. Curran Associates, Inc.
- Lloyd, S. 1982. "Least Squares Quantization in PCM." *IEEE Transactions on Information Theory / Professional Technical Group on Information Theory* 28 (2): 129–37.
- Long, Jonathan, Evan Shelhamer, and Trevor Darrell. 2015. "Fully Convolutional Networks for Semantic Segmentation." In *Proceedings of the IEEE Conference on Computer Vision and Pattern Recognition*, 3431–40.
- Lopez, A. M., F. Llumbreras, J. Serrat, and J. J. Villanueva. 1999. "Evaluation of Methods for Ridge and Valley Detection." *IEEE Transactions on Pattern Analysis and Machine Intelligence* 21 (4): 327–35.
- Lucchi, Aurélien, Kevin Smith, Radhakrishna Achanta, Graham Knott, and Pascal Fua. 2012. "Supervoxel-Based Segmentation of Mitochondria in Em Image Stacks with Learned Shape Features." *IEEE Transactions on Medical Imaging* 31 (2): 474–86.
- Luengo, Imanol, Michele C. Darrow, Matthew C. Spink, Ying Sun, Wei Dai, Cynthia Y. He, Wah Chiu, et al. 2017. "SuRVoS: Super-Region Volume Segmentation Workbench." *Journal of Structural Biology* 198 (1): 43–53.
- Maheshwary, P., and N. Srivastav. 2008. "Retrieving Similar Image Using Color Moment Feature Detector and K-Means Clustering of Remote Sensing Images." In *2008 International Conference on Computer and Electrical Engineering*, 821–24.
- Malakar, Annesha, and Joydeep Mukherjee. 2013. "Image Clustering Using Color Moments, Histogram, Edge and K-Means Clustering." *International Journal of Science and Research* 2 (1): 532–37.
- Malpica, N., C. O. de Solórzano, J. J. Vaquero, A. Santos, I. Vallcorba, J. M. García-Sagredo, and F. del Pozo. 1997. "Applying Watershed Algorithms to the Segmentation of Clustered Nuclei." *Cytometry* 28 (4): 289–97.
- McInerney, T., and D. Terzopoulos. 1996. "Deformable Models in Medical Image Analysis: A Survey." *Medical Image Analysis* 1 (2): 91–108.
- Niculescu-Mizil, Alexandru, and Rich Caruana. 2005. "Predicting Good Probabilities with Supervised Learning." *Proceedings of the 22nd International Conference on Machine Learning - ICML '05*. <https://doi.org/10.1145/1102351.1102430>.
- Platt, John, and Others. 1999. "Probabilistic Outputs for Support Vector Machines and Comparisons to Regularized Likelihood Methods." *Advances in Large Margin Classifiers* 10 (3): 61–74.

- Ren, and Malik. 2003. "Learning a Classification Model for Segmentation." In *Proceedings Ninth IEEE International Conference on Computer Vision*, 10–17 vol.1.
- Ronneberger, Olaf, Philipp Fischer, and Thomas Brox. 2015. "U-Net: Convolutional Networks for Biomedical Image Segmentation." In *Medical Image Computing and Computer-Assisted Intervention – MICCAI 2015*, 234–41. Springer International Publishing.
- Stutz, David, Alexander Hermans, and Bastian Leibe. 2018. "Superpixels: An Evaluation of the State-of-the-Art." *Computer Vision and Image Understanding: CVIU* 166: 1–27.
- "Superpixels – IVRL." n.d. Accessed May 15, 2020. <http://ivrl.epfl.ch/research/superpixels>.
- Vartak, N., G. Guenther, F. Joly, and A. Damle-Vartak. 2019. "Intravital Multi-Modal Flux Analysis Reveals the Transport Mechanism of Bile Acids through Hepatic Microconduits." *bioRxiv*. <https://www.biorxiv.org/content/10.1101/778803v1.abstract>.

Supporting Information (SI) for publication:

Guided interactive image segmentation using machine learning and color based data set clustering

Superpixel features

The superpixel features comprise local and neighborhood color histograms, the averaged gradient magnitude and Laplacian of Gaussian for several sigmas, as well as texture descriptors. Histograms are calculated independently for the red, green and blue channel with each histogram having 16 bins, thus representing 4096 colors. For local histograms all pixels of a superpixel are taken into account. The neighborhood histograms additionally account for all pixels of all neighboring superpixels, thereby providing context. As a means for isotropic edge detection the gradient magnitude is computed separate for the red, green and blue channel after applying gaussian smoothing with variable sigma (0.5, 1, 2, 4, 7, 10). By varying sigma, edges of different scales are accentuated. The gradient magnitude is averaged over all pixels of a superpixel per color channel and sigma. As a second edge detection method based on the second derivative the Laplacian of Gaussian (LoG) is computed for each of the color channels and with variable sigma. The LoG is averaged over all pixels of a superpixel per color channel and sigma. Additionally, a set of six texture describing features is computed. Therefore, the RGB image is converted to a grey-level image which corresponds to the luma component Y of the YIQ color space. Based on this a grey-level co-occurrence matrix is computed which is then used to calculate the texture features (Haralick 1979). Subsequently a texture feature subset comprising Inertia, Cluster Shade, Cluster Prominence, Inverse Difference Moment, Energy and Entropy as proposed by (Conners, Trivedi, and Harlow 1984) is computed.

In summary, the mentioned features constitute a feature vector of 48 entries per local and neighborhood color histograms each, 18 entries per gradient magnitude and LoG values each as well as six texture descriptor entries, yielding a feature vector with a total of 138 entries to characterize each superpixel.

Validation

Gold standard nuclei annotations are given as (center) points. True positive (tp), false positive (fp) and false negative (fn) are quantified based on a object-wise mapping of gold standard to segmentation result. A segmented nucleus is considered a tp, if a gold standard nucleus, thus its 2D coordinate, is inside the segmented area. Accordingly, a segmented nucleus for which no gold standard nucleus exists that is within its confines is considered a fp. A fn nucleus is registered, if there is no segmented nucleus in the immediate neighborhood (kernel of size 1) of a gold standard nucleus.

Performance evaluation

We analyzed the influence of image size and superpixel number on execution times. In the first scenario the image size is successively upscaled from a 1250 x 1250 pixel image to a 15k x 15k pixel image yielding a 144 fold increase in pixel number while working with a constant number of 100k superpixels. The second scenario image size remains constant with 5000 x 5000 pixels but the number of superpixels increases stepwise from 110,835, resulting from superpixels with a target size of 15 x 15 pixels, to 4,471,427, resulting from superpixels of size 2 x 2 pixels, yielding an increase by a factor of 40.3. We evaluated for each scenario runtime of the interactive steps training, prediction and segmentation. Training used in all instances the same (scaled) training masks. Random Forest without optimization and calibration was used as classifier. The analysis was done on a Intel Core i9-7900X with 10 logical cores at a 3.3 GHz clockspeed with 64 GB RAM.

Trivially, the complexity of the training step which maps the user provided training masks to superpixels and compiles the training database from those is independent from the number of pixels. The linear increase by a factor of approx. 2.6 from smallest to largest image shown in Fig 2 can be attributed to linearly increasing image loading times. Similarly, prediction, which encompasses learning and application of the classifier to each superpixel of the image, is independent of image size as it operates directly on superpixel level. The fluctuations seen in Fig 1 between 4.8 sec and 11.41 sec are due to differences in classifier parameterization arising during learning. Segmentation is of linear complexity regarding image size, which is confirmed showing an increase by a factor of 27.9 from 3.8 sec for the smallest to 106.1 sec for the largest image.

Complexity of training, prediction and segmentation is linear in the number of superpixels due to sequential processing, which is confirmed in Fig 2. Training times increase 28.1 fold from 3.9 sec to 109.8 sec, prediction times increase 23.5 fold from 7.9 sec to 185.6 sec and segmentation processing times increase 9.8 fold from 17.6 sec to 171.6 sec.

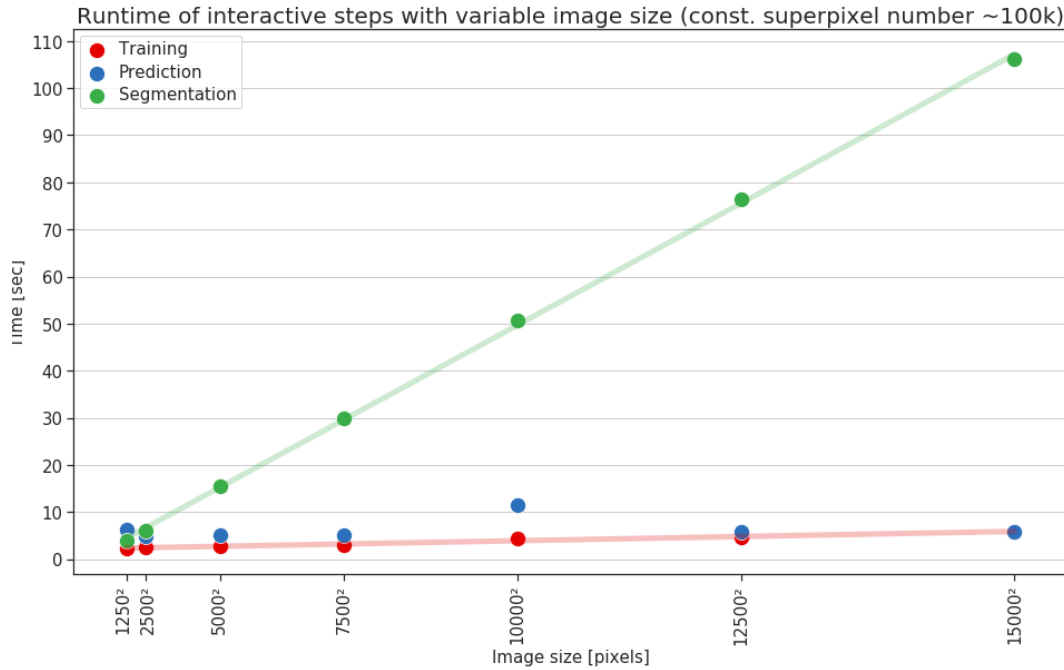


Figure 1: Effect of image size on runtime of interactive processing steps. The training procedure involves identification of annotated superpixels and compilation of the training database. Prediction encompasses fitting of the classifier and prediction of class-membership probabilities for all superpixels of the image. In the segmentation step the final image is produced given the prediction results, no post-processing such as size thresholding, smoothing or watershed is applied. In all instances the same set of training annotations was used, scaled to the respective image size.

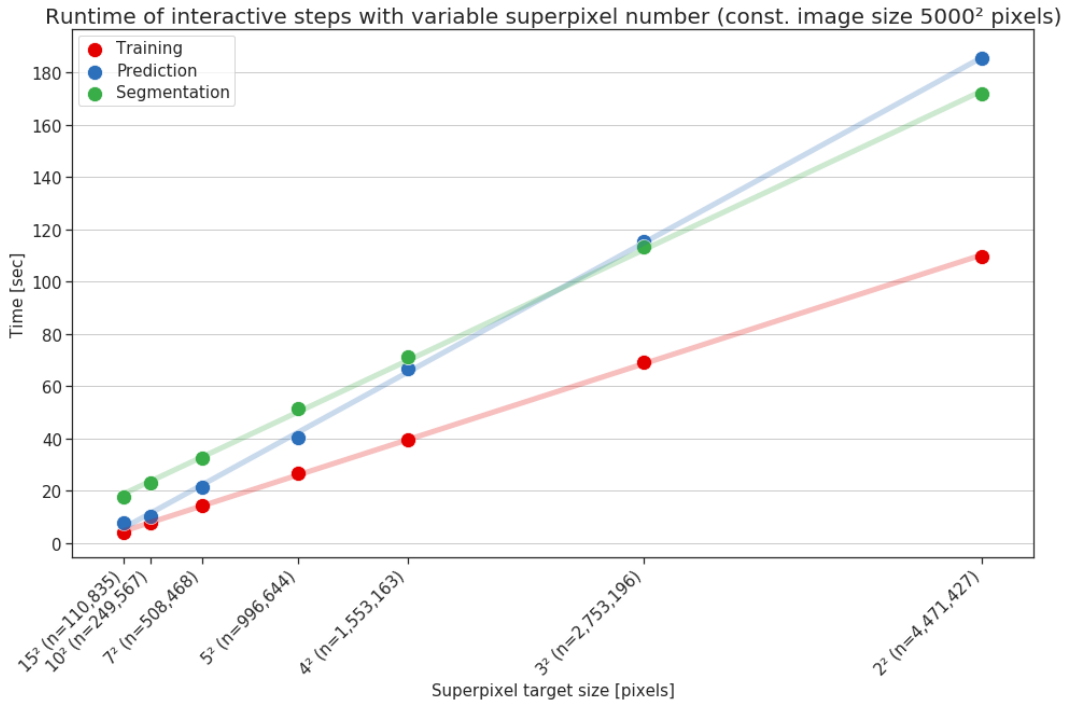


Figure 2: Effect of number of superpixels on runtime of interactive processing steps. In all instances the same set of training annotations was used.

Bibliography

- Achanta, Radhakrishna, Appu Shaji, Kevin Smith, Aurelien Lucchi, Pascal Fua, and Sabine Süsstrunk. 2012. “SLIC Superpixels Compared to State-of-the-Art Superpixel Methods.” *IEEE Transactions on Pattern Analysis and Machine Intelligence* 34 (11): 2274–82.
- Connors, Richard W., Mohan M. Trivedi, and Charles A. Harlow. 1984. “Segmentation of a High-Resolution Urban Scene Using Texture Operators.” *Computer Vision, Graphics, and Image Processing* 25 (3): 273–310.
- Haralick, R. M. 1979. “Statistical and Structural Approaches to Texture.” *Proceedings of the IEEE*. <https://doi.org/10.1109/proc.1979.11328>.